generating 4.8×10^{-18} W per molecule (*31*). The reason that the synthetic system can do more work than the biomolecular one is that kinesin uses adenosine triphosphate as an energy source, which upon hydrolysis releases ~12 kcal mol^{-1}, whereas the present shuttle uses a 355-nm photon of 81 kcal mol^{-1}.

Tuning of the binding properties of the macrocycle and/or stations, and the photophysical properties of the active chromophore, may allow the use of light of a longer wavelength, faster switching times, and/or more powerful and efficient analogs to be produced. Practical applications of such light-induced mechanical motion at the molecular level might involve the rearrangement of the structure of surfaces or the "fetching-and-carrying" of molecules or clusters of atoms between specific locations (for example, across membranes).

References and Notes

1. For examples, see (*2–5*).
2. V. Balzani, A. Credi, F. M. Raymo, J. F. Stoddart, *Angew. Chem. Int. Ed.* **39**, 3348 (2000).
3. J. K. Gimzewski *et al.*, *Science* **281**, 531 (1998).
4. T. R. Kelly, H. De Silva, R. A. Silva, *Nature* **401**, 150 (1999).
5. N. Koumura, R. W. J. Zijlstra, R. A. van Delden, N. Harada, B. L. Feringa, *Nature* **401**, 152 (1999).
6. J.-P. Sauvage, C. Dietrich-Buchecker, Eds., *Molecular Catenanes, Rotaxanes and Knots* (Wiley-VCH, Weiheim, Germany, 1999).
7. For examples, see (*8–13*).
8. R. A. Bissell, E. Córdova, A. E. Kaifer, J. F. Stoddart, *Nature* **369**, 133 (1994).
9. J.-P. Collin, P. Gaviña, J.-P. Sauvage, *New J. Chem.* **21**, 525 (1996).
10. H. Murakami, A. Kawabuchi, K. Kotoo, M. Kunitake, N. Nakashima, *J. Am. Chem. Soc.* **119**, 7605 (1997).
11. A. S. Lane, D. A. Leigh, A. Murphy, *J. Am. Chem. Soc.* **119**, 11092 (1997).
12. N. Armaroli *et al.*, *J. Am. Chem. Soc.* **121**, 4397 (1999).
13. P. R. Ashton *et al.*, *Chem. Eur. J.* **6**, 3558 (2000).
14. For photoresponsive shuttles, see (*10*, *12*, *13*). For reviews of photoresponsive rotaxanes in general, see A. C. Benniston [*Chem. Soc. Rev.* **25**, 427 (1996)] and M.-J. Blanco *et al.* [*Chem. Soc. Rev.* **28**, 293 (1999)].
15. Some supramolecular complexes that are dethreaded by light have been described as "pistonlike. . . light-fueled motors"; see P. R. Ashton *et al.*, *J. Am. Chem. Soc.* **120**, 11190 (1998); M. Asakawa *et al.*, *Chem. Eur. J.* **5**, 860 (1999).
16. D. A. Leigh, A. Murphy, J. P. Smart, A. M. Z. Slawin, *Angew. Chem. Int. Ed. Engl.* **36**, 728 (1997).
17. Details of crystallographic structures are given in the supplementary material (*32*).
18. A. Niemz, V. M. Rotello, *Acc. Chem. Res.* **32**, 44 (1999).
19. "Co-conformation" refers to the relative positions and orientations of the mechanically interlocked components with respect to each other [M. C. T. Fyfe *et al.*, *Angew. Chem. Int. Ed. Engl.* **36**, 2068 (1997)].
20. Details of the CV behavior of **1** and **2** can be found in the supplementary material (*32*).
21. Y. Ge, R. R. Lilienthal, D. K. Smith, *J. Am. Chem. Soc.* **118**, 3976 (1996).
22. G. A. Jeffrey, *An Introduction to Hydrogen Bonding* (Oxford Univ. Press, New York, 1997).
23. Further physical and spectroscopic evidence that rule out folding being the dominant photoinduced process occurring in **1** are provided as supplementary material (*32*).
24. Selective photoexcitation with the third harmonic of a Q-switched Nd:yttrium-aluminum-garnet laser (355 nm, FWHM = 2 ns) of the *ni*-chromophore in **2** leads to the prompt appearance of the triplet-triplet absorption, with characteristic peaks at 369, 441 (shoulder), and 467 nm in MeCN. The decay of the triplet is nonexponential but becomes nearly monoexponential when using the lowest possible laser power on a dilute sample. Under these conditions, the triplet state has a decay time of 43 μs in MeCN. The time resolution of our transient absorption setup (5 ns) does not allow for the detection of the short-lived singlet state. Time-correlated single photon counting, however, afforded a value for the fluorescence decay time of τ_f = 1.6 ns (MeCN).
25. V. Wintgens *et al.*, *J. Chem. Soc. Faraday Trans.* **90**, 411 (1994).
26. Proof of the linear relation between λ_{max} and the intensity of the separate bands when $\Delta\lambda$ is small compared with the width of the separate bands can be found in the supplementary material (*32*).
27. D. A. Leigh, A. Troisi, F. Zerbetto, *Angew. Chem. Int. Ed.* **39**, 350 (2000).
28. D. H. Waldeck, *Chem. Rev.* **91**, 415 (1991).
29. K. M. Omberg *et al.*, *J. Am. Chem. Soc.* **119**, 7013 (1997).
30. X. Y. Lauteslager, I. H. M. van Stokkum, H. J. van Ramesdonk, A. M. Brouwer, J. W. Verhoeven, *J. Phys Chem. A* **103**, 653 (1999).
31. S. M. Block, *Cell* **93**, 5 (1998).
32. Supplementary material is available on *Science* Online at www.sciencemag.org/cgi/content/full/1057886/DC1.

33. This work was supported by the Training and Mobility of Researchers initiative of the European Union through contract FMRX-CT97-0097 (Development of Rotaxane-based Unconventional Materials Network), the Netherlands Organization for Scientific Research (Nederlandse Organisatie voor Wetenschappelijk Onderzoek, NWO) and the Engineering and Physical Sciences Research Council (EPSRC). D.A.L. is an EPSRC Advanced Research Fellow (AF/982324); F.G.G. is a Marie Curie Research Fellow (ERBFMBI-CT97-2834).

29 November 2000; accepted 13 February 2001
Published online 22 February 2001;
10.1126/science.1057886
Include this information when citing this paper.

Tropical Tropospheric Ozone and Biomass Burning

Anne M. Thompson,[1,2]* Jacquelyn C. Witte,[1,4] Robert D. Hudson,[2] Hua Guo,[3] Jay R. Herman,[1] Masatomo Fujiwara[5]

New methods for retrieving tropospheric ozone column depth and absorbing aerosol (smoke and dust) from the Earth Probe–Total Ozone Mapping Spectrometer (EP/TOMS) are used to follow pollution and to determine interannual variability and trends. During intense fires over Indonesia (August to November 1997), ozone plumes, decoupled from the smoke below, extended as far as India. This ozone overlay a regional ozone increase triggered by atmospheric responses to the El Niño and Indian Ocean Dipole. Tropospheric ozone and smoke aerosol measurements from the Nimbus 7 TOMS instrument show El Niño signals but no tropospheric ozone trend in the 1980s. Offsets between smoke and ozone seasonal maxima point to multiple factors determining tropical tropospheric ozone variability.

Smoke and excess tropospheric ozone, both by-products of biomass burning, have long been observed over large regions of the tropics with satellites (*1–3*), aircraft, balloons, and ground-based instrumentation (*4–6*). Ozone forms as a result of biomass burning because combustion products are ozone precursors in the atmosphere: nitrogen oxides, carbon monoxide, and hydrocarbons. Other combustion products lead to the formation of aerosol particles, including soot, that make up smoke. The highest smoke aerosol and tropospheric ozone amounts occur over southern Africa and the adjacent Atlantic (*2*, *5*, *7*), where a strong ozone, biomass-burning link has been confirmed by airborne and ship-based measurements (*5*, *8–11*). However, other observations (*12*) and some models (*13–15*) point to large-scale dynamics and lightning as prominent factors in tropical tropospheric ozone distributions.

Since late 1996, with the launch of Earth Probe–Total Ozone Mapping Spectrometer (EP/TOMS) (*16*), real-time processing of absorbing aerosol (smoke) and tropospheric ozone has enabled daily tracking of these pollutants at 1° latitude by 1.25° longitude resolution. The first exceptional ozone episode detected by EP/TOMS occurred during the 1997 El Niño–Southern Oscillation (ENSO) and Indian Ocean Dipole (IOD) events, when drought over Indonesia was followed by large fires. Here, we use climatological indices to show that ozone variations during this time resulted from perturbed dynamics, as well as from more active photochemistry (*17–21*). Comparison of the EP/TOMS record with data from the Nimbus 7/TOMS instrument that operated from 1979 to 1992 (*7*) shows similarities to data from 1997 and allows determination of seasonal

[1]NASA–Goddard Space Flight Center, Code 916, Greenbelt, MD 20771, USA. [2]Department of Meteorology and [3]Department of Computer Sciences, University of Maryland, College Park, MD 20742, USA; [4]Science Systems and Applications, Lanham, MD 20706, USA; [5]Graduate School of Environmental Earth Science, Hokkaido University, Sapporo 060-0810, Japan.

*To whom correspondence should be addressed: E-mail: anne.m.thompson@gsfc.nasa.gov

cycles in tropospheric ozone and aerosols. The earlier record reveals an offset in the timing of seasonal tropospheric ozone and aerosol maxima and the absence of an ozone trend.

The TOMS smoke aerosol index (*22*, *23*) is used as a proxy for biomass burning because it has daily global coverage and more consistent calibration and sampling than satellite fire counts. Tropospheric ozone column depth (TTO, in Dobson units; 1 DU = 2.69×10^{16} molecules cm^{-2}) (*7*, *24–26*) is retrieved by means of the modified-residual method with corrections for aerosol interferences in total ozone (*27*). Variations in ozone and smoke aerosol over the Indonesian region from August 1996 through December 1998 show a sharp TTO increase in mid-March 1997 (shift from the black to the red line in Fig. 1A), well before biomass fires (dashed line, Fig. 1A) led to a second increase in August 1997 (*28*). The March TTO increase is associated with the 1997–1998 ENSO (Fig. 1B, red triangles) and concurrent IOD that modify wind fields and precipitation (*29–31*). During an IOD event, followed by the Dipole Mode Index (Fig. 1B, asterisks), anomalous subsidence brings ozone toward the surface, causing the column amount to increase. By mid-July, reduced precipitation [elevated outgoing longwave radiation (Fig. 1B, squares)] led to drought conditions over Indonesia and an outbreak of wildfires (*21*).

Ozone and smoke aerosol vary greatly, and not always in phase, during the most intense burning (late July to early November 1997) (Fig. 1A). Six phases in the relation between smoke aerosol and TTO are distinguished, beginning with aerosol and ozone increasing together (Phase 1, Fig. 1C) as photochemical reactions take place among ozone precursors emitted by the fires (*32–34*). Phase 2 is marked by an aerosol increase and an ozone decline. This decoupling results from transport of ozone and smoke aerosol in different layers, a phenomenon suggested by Kita *et al.* (*35*), but not detectable in their analysis. There are several reasons why smoke aerosol and ozone and other trace gases sometimes diverge during the fires. In layers where TOMS detects dense aerosol, ozone may be depleted owing to heavy smoke (*36*). This can be seen during 19 to 27 August 1997, when smoke aerosol stagnates over the Kalimantan (Indonesia) fires (Fig. 2A) while high ozone spreads across western Indonesia and north toward southeast Asia. Evidently, during Phase 2, smoke aerosol was concentrated at ~2 km (750 hPa), and ozone peaks are above where the reflecting smoke layer causes an increase in the rates of ozone-forming photochemical reactions (*20*). Forward trajectories initialized with an air-parcel model (*37*) from the location of Kalimantan fires (black lines, Fig. 2A) show slow transport of aerosol. Ozone (Fig. 2B) follows faster 3-km (southerly) and 6-km (easterly) pathways. Southerly transport of ozone at 3 to 4 km is confirmed by the 27 August 1997 sounding at Watukosek, Java (*17*) (Fig. 2C).

Phase 3, occurring in the first half of September (Fig. 1C), marks a rapid increase in both smoke and TTO, brought on by heavy burning over Kalimantan and Sumatra and, to a lesser extent, over New Guinea (black contour in Fig. 3A). Forward trajectories at 3 and 6 km (*37*) (Fig. 3A) during this phase indicate recirculation over the Indonesian maritime continent that allows smoke to accumulate and TTO to reach 70 DU by 15 September. TTO during Phases 4 and 5 (Fig. 1C) is 10 to 30 DU above the Indonesian average (dashed line in Fig. 4A), similar to model calculations (*20*) and to excess ozone reported by the Global Ozone Monitoring Experiment satellite (*38*). Phase 4 (Fig. 1C) shows TTO and smoke decoupled. Here, aerosol builds up in the boundary layer until there is a lull in fires during the last week of September. At 3 to 6 km, where ozone is concentrated (*17*), increased winds transport ozone to the Indian Ocean (Fig. 3B) and maximum TTO drops to 50 DU. Ozone maximizes in Phase 5 when fires pick up again after 10

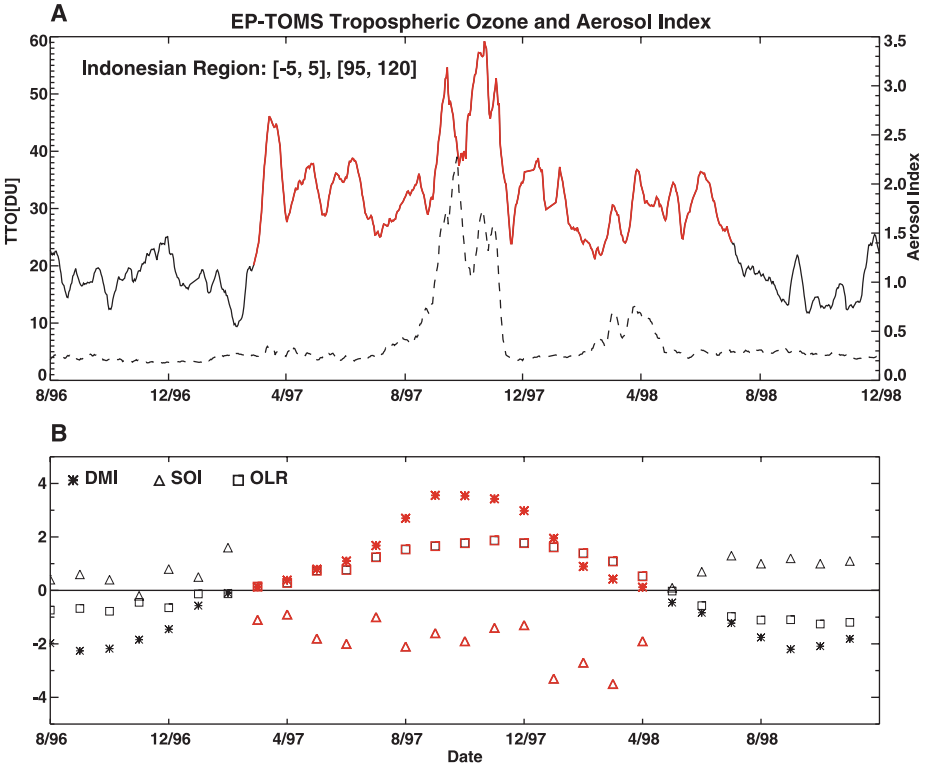

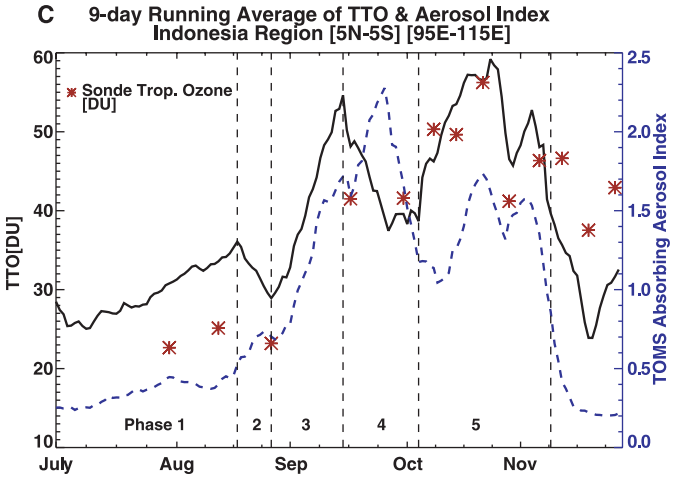

Fig. 1. (**A**) Time series of tropospheric ozone (solid line) from the modified-residual method (*7*) as observed by EP/TOMS from August 1996 through December 1998. Nine-day running means are used with 1° by 1.25° gridded data averaged over 5N-5S, 95-120E. Nine-day running means of smoke aerosol index (dashed line) are also shown. (**B**) SOI (from the National Centers for Environmental Prediction Climate Prediction Center; www.cpc.ncep.noaa.gov/data/indices/). The DMI (*30*, *31*) is from http://w3.frontier.esto.or.jp/d1/saji/saji.html. (**C**) Expanded scale of TTO (solid black) and smoke aerosol (dashed blue) during the most intense wildfires in 1997. Stars signify integrated tropospheric ozone column amounts from ozonesondes (*17*) at Watukosek (Java, 7.5°S, 113°E). Phases are described in the text.

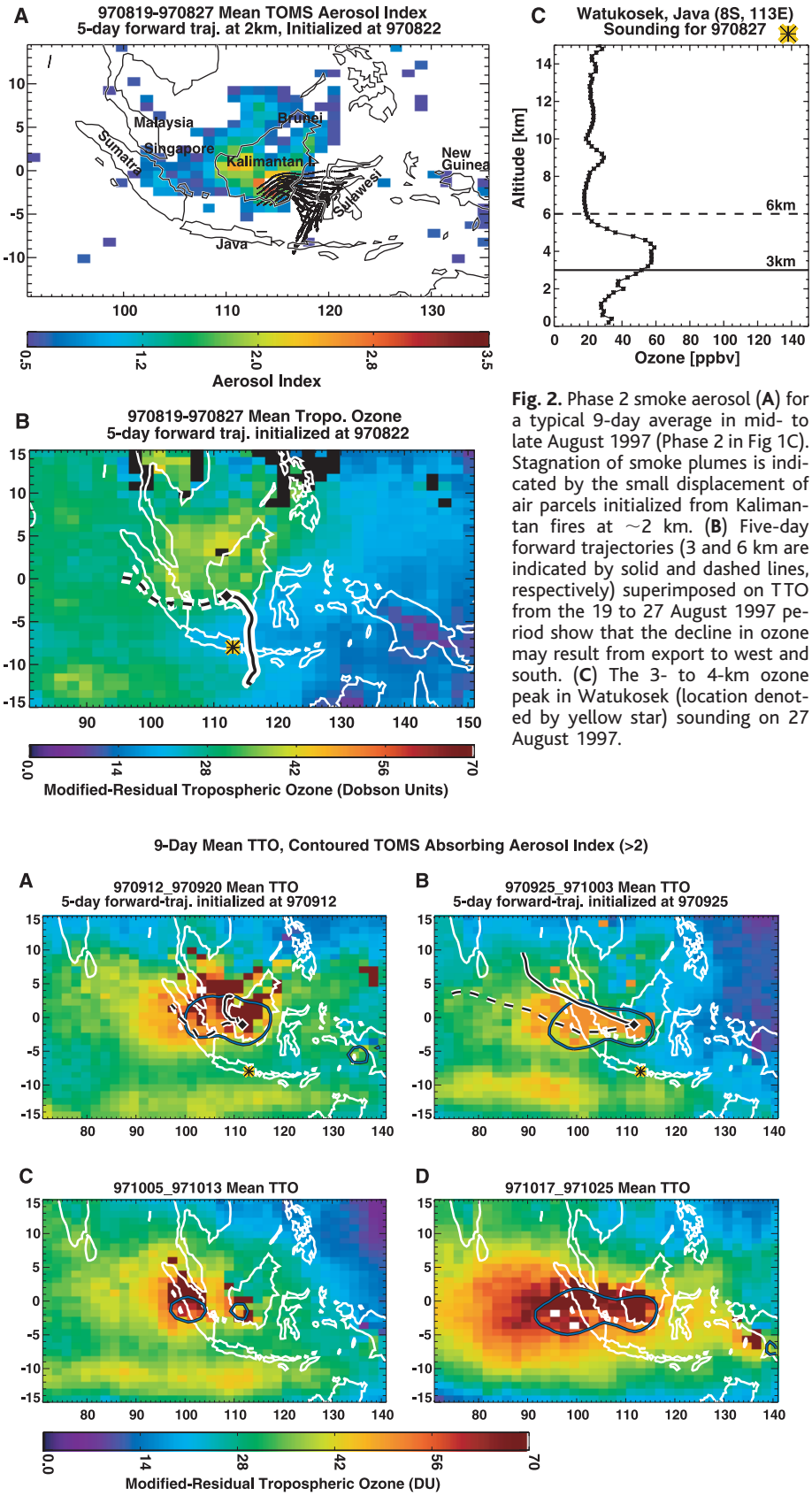

Fig. 2. Phase 2 smoke aerosol (**A**) for a typical 9-day average in mid- to late August 1997 (Phase 2 in Fig 1C). Stagnation of smoke plumes is indicated by the small displacement of air parcels initialized from Kalimantan fires at ~2 km. (**B**) Five-day forward trajectories (3 and 6 km are indicated by solid and dashed lines, respectively) superimposed on TTO from the 19 to 27 August 1997 period show that the decline in ozone may result from export to west and south. (**C**) The 3- to 4-km ozone peak in Watukosek (location denoted by yellow star) sounding on 27 August 1997.

Fig. 3. (**A**) High smoke aerosol (contoured where the index > 2) and TTO. (**B**) Phase 3 (Fig. 1C) with declining ozone in late September 1997. Forward trajectories superimposed over ozone at 3 (solid line) and 6 km (dashed line). In late September through early October, TTO declines when ozone flows from Kalimantan toward Singapore, Malaysia, and the Indian Ocean. (**C** and **D**) Maximum TTO is attained in Phase 5, and the plume extends to Sri Lanka and southern India.

October (Fig. 3C). By late October 1997, three distinct plumes—from Kalimantan-Sumatra-Malaysia, Africa (high TTO, 10° to 15°S) (Fig. 3, A to C), and New Guinea—merge into a single feature extending to Sri Lanka and India (Fig. 3D). Ozone soundings verify that free tropospheric ozone increases in layers of varying intensity and thickness during October to November (*17*). Some ozone precursors reach 9 to 12 km (*34*), but ozone above this altitude is of uncertain origin. The sharp TTO drop in early November 1997 (Fig. 1C) marks a return to typical values for that time of year (Fig. 5).

The positive relation between anomalously high Indonesian ozone and Southern Oscillation (SOI) and Dipole Mode Index (DMI) also appears in the 1979 to 1992 Nimbus 7 TOMS record (*7*, *29*). The 1982–1983 ENSO and IOD begin with low ozone (TTO ~20 DU) (Fig. 4A), followed by an ozone jump when SOI and DMI increase. A second ozone increase accompanies enhanced fire activity (Fig. 4B). The TTO and smoke aerosol 1980–1990 time series show no statistically significant trend (*39*–*42*) over Indonesia or other regions (South America and Africa) where biomass burning is an important contributor to ozone formation (*7*). The lack of a tropospheric ozone trend is consistent with recent work (*43*, *44*) that indicates no TOMS total ozone change in the tropics during 1979–1992.

Further examination of the ozone-smoke relation shows a general tendency for tropical ozone and smoke aerosol to be decoupled. The statistical model (*39*) used for analysis of 1980–1990 trends also yields the annual cycle in tropospheric ozone and smoke aerosol (Fig. 5). The regions selected straddle the equator so that both Northern and Southern Hemisphere burning seasons are captured. North of the equator biomass fires typically peak between December and April. To the south, fires peak between July and November. In none of the three regions illustrated is there a straightforward relation between the ozone maximum and peak burning. This is most evident over equatorial Africa, where the highest burning signal (January aerosol maximum) does not correspond to the highest ozone (*45*). In all cases, maximum TTO occurs in September to October. Only over South America does this match local burning, and even there, the shoulder of high ozone that occurs in July to August probably denotes ozone transported from Africa (*4*, *5*). Besides intercontinental transport, offsets have been attributed to interhemispheric transport, lightning, and large-scale dynamics (*10*, *12*–*15*). Whatever the case, the inference is that biomass burning, although critical during intense episodes, is only one factor determining the tropospheric ozone column in the tropics.

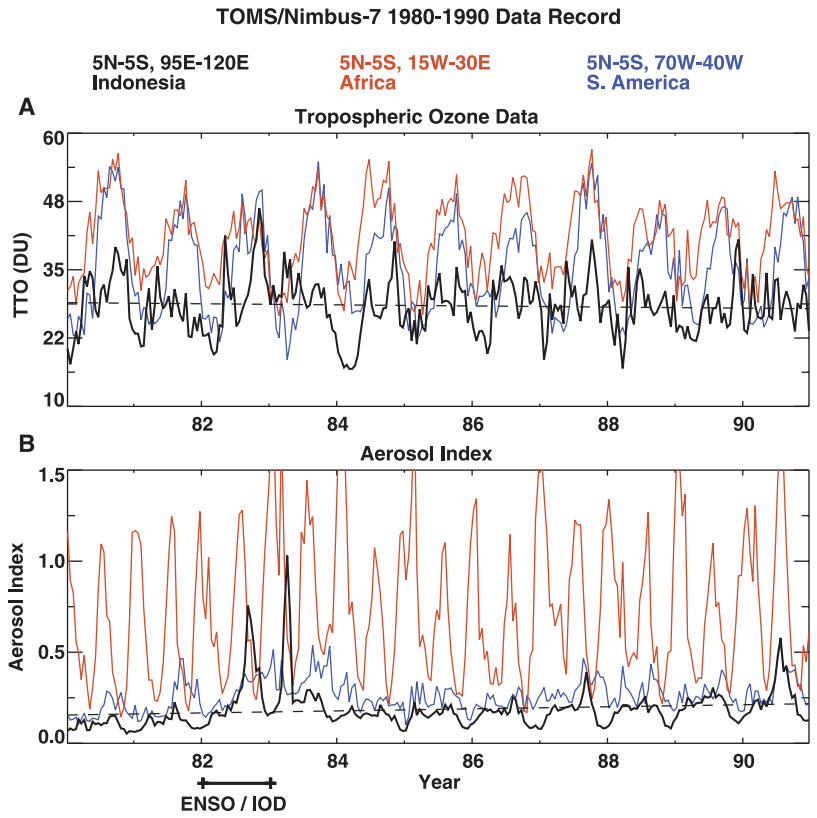

Fig. 4. (**A**) Tropospheric ozone and (**B**) smoke aerosol, averaged twice monthly from the Nimbus 7/TOMS instrument for three regions. Dashed lines represent deseasonalized trends from 1980 to 1990, not statistically significant in TTO. The apparent increase in smoke aerosol may be an artifact of instrument drift (*41*); smoke increases in the 1990s are more likely (*42*). Trend calculations for Africa and South America (not shown) also show no ozone trend (*7*).

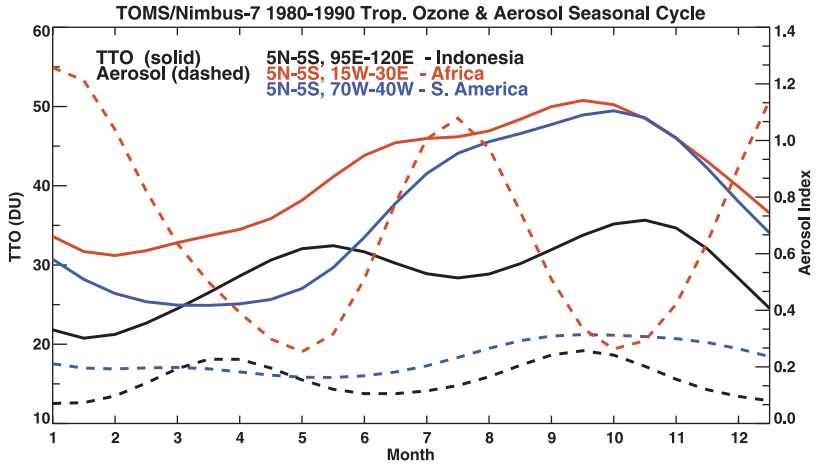

Fig. 5. Seasonal cycle based on 1980–1990 Nimbus 7/TOMS TTO and smoke aerosol, derived from the same statistical model (*39*) used in Fig 4.

References and Notes

1. Smoke is detected from a number of satellite sensors, e.g., AVHRR (Advanced Very-High Resolution Radiometer), GOES (Geostationary Observations over Earth Sensor), SeaWIFS (Sea Wide-Field of View Spectrometer), TOMS, and MODIS (Moderate High-Resolution Imaging Spectrometer). Fires are detected from some satellites. See fire counts from Along-Trace Scanning Radiometer (ATSR) at http://shark1.esrin.esa.it/FIRE/AF/ATSR. In the present study, a generally good colocation of TOMS smoke aerosol and ATSR fires in August to October 1997 allows use of TOMS aerosol as a proxy for burning activity. Fishman and Brackett (*2*) give 2- to 3-month-averaged tropospheric ozone obtained by subtraction of the SAGE (Stratospheric Aerosols and Gases Experiment) satellite instrument stratospheric column ozone from TOMS total ozone. Attempts to extract daily tropospheric ozone by subtracting solar backscatter ultraviolet stratospheric column ozone from TOMS may give erroneous results (*3*).
2. J. Fishman, V. G. Brackett, *J. Geophys. Res.* **102**, 19275 (1997).
3. J. R. Ziemke, S. Chandra, *J. Geophys. Res.* **103**, 13903 (1998).
4. V. W. J. H. Kirchhoff *et al.*, *J. Geophys. Res.* **96**, 10899 (1991).
5. A. M. Thompson *et al.*, *J. Geophys. Res.* **101**, 24251 (1996).
6. F. G. Taupin, M. Bessafi, S. Baldy, P. J. Bremaud, *J. Geophys. Res.* **104**, 8057 (1999).
7. A. M. Thompson, R. D. Hudson, *J. Geophys. Res.* **104**, 26961 (1999).
8. M. O. Andreae *et al.*, *J. Geophys. Res.* **99**, 12793 (1994).
9. D. J. Jacob *et al.*, *J. Geophys. Res.* **101**, 24235 (1996).
10. I. Jonquières, A. Marenco, A. Maleej, F. Rohrer, *J. Geophys. Res.* **103**, 19059 (1998).
11. R. Weller *et al.*, *J. Geophys. Res.* **101**, 1387 (1996).
12. A. M. Thompson *et al.*, *Geophys. Res. Lett.* **27**, 3317 (2000).
13. T. N. Krishnamurti *et al.*, *J. Geophys. Res.* **101**, 23889 (1996).
14. W. L. Moxim, H. Levy II, *J. Geophys. Res.* **105**, 17393 (2000).
15. R. V. Martin *et al.*, *Geophys. Res. Lett.* **27**, 1639 (2000).
16. The operational EP/TOMS instrument was launched in a low-Earth polar orbit (500 km) in July 1996. In August 1996 another TOMS was launched, on board the polar orbiting Advanced Earth Observing Satellite (ADEOS) platform. ADEOS failed in June 1997 and the EP/TOMS orbit was raised in early December 1997, giving a 2-week data gap during the boosting process. The Nimbus 7/TOMS polar orbiting instrument operated from late 1978 through April 1993. Meteor/TOMS flew in a nonpolar orbit from August 1991 through December 1994.
17. M. Fujiwara *et al.*, *Geophys. Res. Lett.* **26**, 2417 (1999).
18. Fujiwara and co-workers (*19*) describe dynamic influences on Indonesian ozone profiles, taken at Watukosek (7.5°S, 113°E). Similar inferences were made about March to May 1997 upper-tropospheric ozone profiles over Malaysia (H. Tsuruta *et al.*, paper presented at the Southeast Asia International Global Atmospheric Chemistry Symposium, 22 to 23 January 2001, Bangkok, Thailand).
19. M. Fujiwara *et al.*, *J. Geophys. Res.* **105**, 1879 (2000).
20. D. A. Hauglustaine, G. P. Brasseur, J. S. Levine, *Geophys. Res. Lett.* **26**, 3305 (1999).
21. M. J. Wooster, R. Ceccato, and S. P. Flasse [*Int. J. Remote Sens.* **19**, 383 (1998)] show AVHRR-derived smoke and fires in September 1997.
22. The TOMS aerosol index [(*23*); data at http://toms.gsfc.nasa.gov] is approximately the difference in reflectivity between two wavelengths (340 to 380 nm or 331 to 360 nm) and is sensitive to ultraviolet-absorbing particles at ~2 km and above. When converted to optical depth, the sensitivity extends to the surface.
23. J. R. Herman *et al.*, *J. Geophys. Res.* **102**, 16911 (1997).
24. The modified-residual method is valid only in air masses identified as tropical by a wave-one pattern in total ozone (*25*) and in air masses free of high reflectivity. The technique and error analysis are described in (*7*) and (*25*). Time averaging is used to eliminate scan-angle biases in Level 2 TOMS data and to correct for low detection efficiency of near-surface ozone (*26*). The reflectivity criterion and retrieval interferences of dense smoke aerosol are handled as follows. No processing is done for pixels with reflectivity >0.15, and total ozone is corrected with the formula of Torres and Bhartia (*27*) before derivation of tropospheric ozone. This leads to some gaps in TTO. For the present analysis, gaps were filled in with the highest TTO value in the 5N to 5°S, 95° to 115°E region. This could be considered a worst-case scenario, with filled-in pixels as an upper limit, or as a conservative choice if gaps signify even higher ozone above concentrated smoke aerosol. Daily TTO data for 1979–1992 (Nimbus 7) and 1996–1999 (Earth Probe) are available at http://metosrv2.umd.edu/~tropo.
25. R. D. Hudson, A. M. Thompson, *J. Geophys. Res.* **103**, 22129 (1998).
26. R. D. Hudson, J.-H. Kim, A. M. Thompson, *J. Geophys. Res.* **100**, 11138 (1995).

27. O. Torres, P. K. Bhartia, *J. Geophys. Res.* **104**, 21569 (1999).
28. Additional maps illustrating the regional TTO increase in March 1997 are at http://metosrv2.umd.edu/~tropo. Animation of superimposed TTO and smoke aerosol from July through October 1997 is available on *Science* Online at www.sciencemag.org/cgi/content/full/291/5511/2128/DC1. The March ozone jump also coincided with a satellite-based upper-tropospheric H_2O decrease (*29*). Unfortunately, there are no H_2O data in the Watukosek soundings to verify the H_2O-ozone relation.
29. S. Chandra, J. R. Ziemke, W. Min, W. G. Read, *Geophys. Res. Lett.* **25**, 3867 (1998).
30. The SOI is defined as a normalized difference of sea-level pressure anomalies between the eastern Pacific (Tahiti) and the Maritime Continent (Darwin). The DMI (Fig. 1B) is an index of the IOD (*31*) that estimates anomalous fluctuations of the equatorial sea-surface temperature (SST) gradient in the Indian Ocean. In the time period of this analysis, ENSO and IOD, two independent phenomena, occur simultaneously. As SST conditions change, there are variations in convection and subsidence (downward motion, negative SOI, and increase in TTO). Outgoing longwave radiation (OLR) is used here as a proxy for deep convection, a positive OLR anomaly signifying less convective activity or rainfall than usual and, consequently, anomalous subsidence. Early March marked the start of an ENSO/IOD event (SOI-negative, DMI-positive, OLR-positive) that reached greatest instensity by October 1997, coincident with maximum TTO. Downward mixing by an equatorial Kelvin wave and the Madden-Julian Oscillation may also enhance TTO over Indonesia during the 1997 fires (*19*).
31. N. H. Saji, B. N. Goswami, P. N. Vinayachandran, T. Yamagata, *Nature* **401**, 360 (1999).
32. Typical ozone-formation rates in savanna-burning regions, 10 to 15 parts per billion by volume of ozone/day in the boundary layer (*5*, *9*, *10*), are equivalent to 2 to 4 DU/day. Although ozone is destroyed at the surface, it may form above the boundary layer after convective transport of ozone precursors. Free tropospheric ozone–formation rates are lower, but ozone persists for several weeks or more (*5*, *9*) and keeps forming as ozone precursors are transported downwind. This is referred to as "mix-then-cook" by Chatfield and Delany (*33*). Alternatively, if ozone formed near the surface is mixed up to the free troposphere, "cook-then-mix" (*33*), it can accumulate in recirculating air parcels. Recirculation may have contributed to high TTO (70 DU) over Indonesia—50 to 60 DU is a typical value over African burning (*7*). On the other hand, ozone photochemical formation over Indonesia may have been greater than over African savanna fires because smoldering combustion near Kalimantan peat bogs produced ozone precursors at a higher rate (*34*). Sampling on a commercial airliner recorded elevated CO concentrations at 8 to 13 km over Indonesia after mid-September 1997. This implies exhalation of the lower troposphere.
33. R. B. Chatfield, A. D. Delany, *J. Geophys. Res.* **95**, 18473 (1990).
34. H. Matsueda, H. Y. Inoue, *Geophys. Res. Lett.* **24**, 2413 (1999).
35. K. Kita, M. Fujiwara, S. Kawakami, *Atmos. Environ.* **34**, 2681 (2000).
36. Y. Tsutsumi *et al.*, *Geophys. Res. Lett.* **26**, 595 (1999).
37. The model used is the isentropic trajectory model of M. R. Schoeberl and P. A. Newman [*J. Geophys. Res.* **100,** 25801 (1995)]. Clusters of trajectories are initialized at the 310 K potential temperature level for the smoke and at 316 and 331 K for the ozone layers. Winds are taken from National Center for Environmental Prediction (NCEP) 2.5° by 2.5° analysis.
38. J. P. Burrows *et al.*, *J. Atmos. Sci.* **56**, 155 (1999). GOME also detected elevated carbon monoxide and formaldehyde.
39. The statistical method used in Figs. 4 and 5 is based on the method described by S. M. Hollandsworth *et al.* [*Geophys. Res. Lett.* **22,** 905 (1995)]. The Nimbus 7 record covers 14 full years, but the start-up year is omitted and 1991–1992 data are not used because of aerosol artifacts after the Mount Pinatubo, Philippines, eruption. No tropical regions displayed a tropospheric ozone trend in the 1980s, according to the modified-residual method (*7*). An alternate technique for deriving TTO from TOMS (*40*) also shows no statistically significant ozone trend in the 1980s. See TTO during the 1982–1983 ENSO at http://metosrv2.umd.edu/~tropo.
40. S. Chandra, J. R. Ziemke, R. W. Stewart, *Geophys. Res. Lett.* **26**, 185 (1999).
41. J. F. Gleason, N. C. Hsu, O. Torres, *J. Geophys. Res.* **103**, 31969 (1998).
42. N. C. Hsu *et al.*, *J. Geophys. Res.* **104,** 6269 (1999).
43. R. D. Hudson, A. D. Frolov, in preparation.
44. There appears to be a trend in total ozone when TOMS data are analyzed by latitude band, but the trend in tropical total ozone disappears when analysis is done within a meteorologically coherent regime (*43*). The lack of a TTO trend (*7*) is not surprising because the modified-residual method is restricted to a meteorologically defined tropical band (*25*).
45. In January 1993 and January 1999, during northern African biomass burning, the highest ozone over the Atlantic was observed south of the Intertropical Convergence Zone (*11*, *12*) a phenomenon designated the "tropical Atlantic paradox." According to Moxim and Levy (*14*), lightning is the dominant tropical NO source except during the southern African burning season.
46. We are grateful to the TOMS Ozone Processing Team for real-time data; S. M. Hollandsworth, T. L. Kucsera, and M. G. Seybold (Science Systems and Applications at NASA-Goddard) for assistance with the regression model; and A. D. Frolov and A. K. Kochhar for work on the University of Maryland Web site. H. Saji generously provided the OLR and DMI. Comments on the manuscript by R. B. Chatfield, J. F. Gleason, R. S. Stolarski, J. P. Burrows, and A. Ladstätter-Weiβmayer are greatly appreciated. Supported by NASA Programs in Atmospheric Chemistry, Modeling and Analysis (ACMAP) and Tropospheric Chemistry.

24 October 2000; accepted 13 February 2001

Synchronous Tropical South China Sea SST Change and Greenland Warming During Deglaciation

M. Kienast,[1]* S. Steinke,[2] K. Stattegger,[2] S. E. Calvert[1]

The tropical ocean plays a major role in global climate. It is therefore crucial to establish the precise phase between tropical and high-latitude climate variability during past abrupt climate events in order to gain insight into the mechanisms of global climate change. Here we present alkenone sea surface temperature (SST) records from the tropical South China Sea that show an abrupt temperature increase of at least 1°C at the end of the last glacial period. Within the recognized dating uncertainties, this SST increase is synchronous with the Bølling warming observed at 14.6 thousand years ago in the Greenland Ice Sheet Project 2 ice core.

Previous studies of the phase relation between tropical and high-latitude warming during the last deglaciation came to contrasting conclusions: the tropical ocean was either synchronous with (*1*) or led (*2*, *3*) the Northern Hemisphere deglacial temperature increase. Antiphasing between changes in tropical Atlantic SST and temperature over Greenland is expected based on the bipolar see-saw mechanism (*4*). But the timing of deglacial SST increases in the Pacific and Indian Oceans relative to high-latitude warming is still controversial. On the basis of a radiocarbon-dated alkenone thermometry (U^K_{37})-SST record from the tropical northwestern Indian Ocean, Bard *et al.* (*1*) inferred an interhemispheric synchrony of deglacial warming in the Arabian Sea and Greenland, specifically during the Bølling Transition at the end of the last glaciation. However, this Indian Ocean U^K_{37}-SST change leads planktonic foraminiferal $\delta^{18}O$ from the same core (*5*) during this abrupt event. A similar lead of foraminiferal Mg/Ca-derived SST estimates versus $\delta^{18}O$, as well as the correspondence between equatorial Pacific foraminiferal Mg/Ca and Antarctic temperature records, however, prompted Lea *et al.* (*2*) to postulate a lead of tropical Pacific deglacial SST increase versus ice volume, and a synchroneity with Antarctic warming during deglaciation.

Here we present two high-resolution, accelerated mass spectrometry (AMS) ^{14}C-dated U^K_{37}-SST and foraminiferal $\delta^{18}O$ records (Fig. 1, A and B) (*6*) from the tropical southern South China Sea (SCS), a non-upwelling environment within the Western Pacific Warm Pool (WPWP), that cover the late glacial–to-Holocene transition. Sediment cores 18252-3 and 18287-3 were retrieved from the southwestern (9°14′N, 109°23′E, 1273-m water depth) and southern (5°39′N, 110°39′E, 598-m water depth) SCS, respectively. According

[1]Earth and Ocean Sciences, University of British Columbia, Vancouver, B.C. Canada V6T 1Z4. [2]Institut für Geowissenschaften, Universität Kiel, Kiel, Germany.

*To whom correspondence should be addressed. E-mail: kienast@unixg.ubc.ca

Tropical Tropospheric Ozone and Biomass Burning

Anne M. Thompson, Jacquelyn C. Witte, Robert D. Hudson, Hua Guo, Jay R. Herman, and Masatomo Fujiwara

Science, **291** (5511), .
DOI: 10.1126/science.291.5511.2128